Available online at www.sciencedirect.com
SCIENCE DIRECT®
Journal of Nuclear Materials 328 (2004) 88–96
journal of nuclear materials
www.elsevier.com/locate/jnucmat

Spectroscopic and microscopic investigation of the corrosion of 316/316L stainless steel by lead–bismuth eutectic (LBE) at elevated temperatures: importance of surface preparation

Allen L. Johnson [a,*], Denise Parsons [a], Julia Manzerova [a], Dale L. Perry [b], Dan Koury [c], Brian Hosterman [c], John W. Farley [c]

[a] *Department of Chemistry, University of Nevada, Las Vegas, 4505 S. Maryland Parkway, P.O. Box 4003, Las Vegas, NV 89154-4003, USA*
[b] *Mail Stop 70A-1150, Lawrence Berkeley National Laboratory, Berkeley, CA 94720, USA*
[c] *Department of Physics, University of Nevada, Las Vegas, 4505 S. Maryland Parkway, P.O. Box 4002, Las Vegas, NV 89154-4002, USA*

Received 7 July 2003; accepted 9 March 2004

Abstract

The corrosion of steel by lead–bismuth eutectic (LBE) is an important issue in proposed nuclear transmutation schemes. Russian scientists at the IPPE exposed steel samples to oxygen-controlled LBE at temperatures up to 823 K and exposure times up to 3000 h. We have characterized these post-exposure steel samples and unexposed controls, using scanning electron microscopy (SEM), energy-dispersive X-ray analysis (EDAX) and X-ray photoelectron spectroscopy (XPS). Previous researchers have investigated the corrosion by LBE of steel of varying composition. In the present work, we compared two samples having the same composition (standard nuclear grade 316/316L) but different surface preparation: a cold-rolled sample was compared with an annealed sample. The cold-rolled sample had an order of magnitude less corrosion (i.e., both lower oxidation and less weight change) than the annealed sample. Sputter depth profiling of the exposed annealed sample and cold-rolled sample showed a marked difference in oxide layer composition between the annealed and cold-rolled samples. The annealed sample showed a complex oxide structure (iron oxide over chromium/iron oxide mixtures) of tens of microns thickness, while the cold-rolled sample was covered with a rather simple, primarily chromium oxide layer of ~1 μm thickness.
Published by Elsevier B.V.

1. Introduction

Lead–bismuth Eutectic (LBE) is of interest as both a coolant and a spallation target in proposed transmutation schemes for radioactive waste. Unfortunately, hot LBE corrodes most engineering materials. Studies of corrosion in the LBE/stainless steel system are important in assessing the feasibility of transmutation plans.

The Russians have decades of experience with LBE as a coolant in their Alpha-class submarines, generating a body of engineering knowledge on the material. They found that the addition of controlled amounts of oxygen to LBE greatly suppressed the corrosion of steel by LBE. The suppression of corrosion is believed to arise from the formation of a protective oxide layer on the metal surface

* Corresponding author. Tel.: +1-702 895 0881; fax: +1-702 895 4072.
E-mail address: aljohnson@ccmail.nevada.edu (A.L. Johnson).

0022-3115/$ - see front matter Published by Elsevier B.V.
doi:10.1016/j.jnucmat.2004.03.006

[1]. The oxide layer passivates the surface, retarding the corrosion rate. In principle, such an oxide layer can be self-healing, because if the oxide layer is disrupted for any reason, a fresh oxide layer would re-form.

The present study of oxide composition and morphology was undertaken in order to understand the corrosion of 316/316L stainless steel in oxygen-controlled LBE, and the anomalously low corrosion rate of a sample of 316/316L stainless steel whose surface has been prepared by cold-rolling.

2. Recent studies of corrosion of steel by LBE

Recent studies of corrosion in the LBE/stainless steel system include the work of Loewen et al. [2], who studied the corrosion of 316L and other steels in a stirred, isothermal LBE bath at 823 and 923 K for 1000 h. Oxide thicknesses of the order 5–33 μm were found.

Benamati et al. [3] reported the results of exposure of two types of stainless steels, AISI 316L (austenitic) and MANET II (martensitic) to stagnant LBE at temperatures of 823 K for times up to 5000 h. In addition, they exposed the Russian ferritic–martensitic stainless steel EP823 to flowing LBE at 823 K for times up to 700 h. Active oxygen control was not employed. In the stagnant test, at temperatures up to 673 K, both AISI 316L and MANET II developed an oxide layer, and exhibited good resistance to oxidation corrosion. However, at a temperature of 823 K, both AISI 316L and MANET II exhibited serious dissolution corrosion. In the flowing LBE test, the EP823 steel exhibited resistance to dissolution, even at temperature of 823 K for 700 h exposure. This resistance is attributed to development of a protective double oxide layer, consisting of an inner layer (probably spinel) of oxygen, chromium, iron and silicon, and an outer layer (probably magnetite) of iron and oxygen.

Müller et al. [4] exposed several types of stainless steel to flowing LBE under active oxygen control. AISI 316L (autenitic), 1.4970 (austenitic) and MANET (martensitic) stainless steels developed stable oxide layers and resisted corrosion at temperatures up to 550 °C for 2000 h. At 600 °C, type 1.4970 was resistant to corrosion while AISI 316L showed massive corrosion. In a separate experiments, aluminum was incorporated in the sample surface, either by hot-dipping the sample in liquid aluminum, or by hot-wrapping the sample in aluminum foil. At a temperature of 600 °C, hot-wrapped samples, either AISI 316L or 1.4970, resisted corrosion, while hot-dipped samples, either AISI 316L or 1.4940, did not resist corrosion.

Fazio et al. [5] reported measurement of corrosion of steel and refractory metals (W, Mo) by oxygen-controlled flowing LBE. After 1500 h of exposure at 673 K, all metals suffered liquid metal attack and showed weight loss. Austenitic and martensitic steels showed comparable corrosion rates, while refractory metals were more resistant than steels. The tensile strengths of austenitic steels were unaffected, while martensitic steels showed a mixed brittle–ductile fracture surface. Glasbrenner et al. [6] studied the tensile strength of MANET II steel after exposure to LBE at temperatures of 453–573 K and times of about two hours. They found no loss of ductility at 473 K, and some loss of ductility at 523 and 573 K. They found penetration of LBE along the grain boundaries. Guerin et al. [7] studied the combined effect of LBE and hydrogenated helium (4% H_2 in He) on T91 steel. Samples were exposed for 12 h to stagnant LBE without oxygen control. They found an oxide film was protective at temperatures up to 573 K, but delamination occurred at temperatures of 623 K and above. Kikuchi et al. [8] reported studies of 316 stainless steel exposed to flowing LBE in the absence of active oxygen control, compared with a sample exposed to stagnant LBE. After 3000 h of exposure at 723 K, the sample exposed to flowing LBE showed mass transfer, roughening of the surface in the high-temperature region, and recrystallization of steel in the low-temperature region.

In these previous studies, steels of different composition were exposed to stagnant or flowing LBE. In some studies, the LBE was oxygen-controlled. The post-exposure steel samples were then characterized. These studies show the importance of the composition of the steel, as well as the exposure time and especially the temperature, in influencing the corrosion rate. What has been lacking in the literature is a study of the importance of surface preparation of the steel, as opposed to the composition of the steel. Since corrosion occurs at the surface, clearly surface preparation could be quite important. This study examines samples of 316 steel with the same composition but different surface preparation (cold-rolled or annealed). The present study is a contribution toward filling this gap in the literature.

3. Experimental

This work was motivated by recent results of Russian researchers [1]. The 316/316L nuclear grade stainless steel samples studied were among a batch of steels corrosion-tested by scientists at the Institute of Physics and Power Engineering (IPPE) in Obninsk, Russia, under contract to Los Alamos National Laboratory (LANL). The steel samples were inserted in IPPE's CU-1M non-isothermal LBE loop for time intervals of 1000, 2000, and 3000 h at temperatures of 733 and 823 K. The oxygen level in the LBE was maintained at 30–50 ppb. The initial concentration of oxygen was set by dissolving BiO in the liquid LBE, and the level was later maintained by electrochemical generation of oxygen. Our particular samples were an 8 mm diameter tube (6 mm

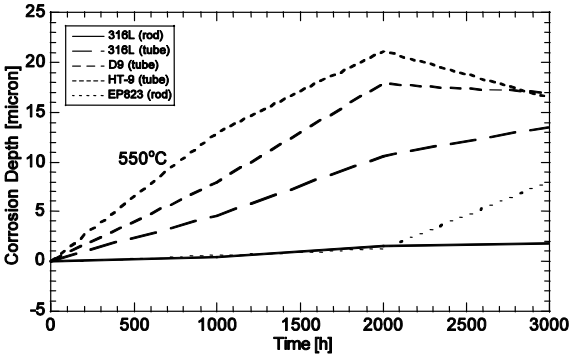

Fig. 1. Corrosion depth as a function of time of exposure to LBE, for different steel samples. Reprinted with permission from Ref. [1b].

ID) of annealed material and 8 mm diameter rod of cold-rolled material.

The Russian collaborators at IPPE measured corrosion depth (i.e., loss of original substrate material, computed from weight change and oxide film thickness) of stainless steel samples after exposure to LBE [1a] and [1b], as shown in Fig. 1 (by permission). They found that the cold-rolled 316/316L rod sample had an *order of magnitude less* corrosion depth than the annealed 316/316L tube steel sample. Even after 3000 h of exposure to LBE at a temperature of 873 K, they found an impervious $\sim$1 μm oxide layer in the favorable (cold-rolled) case. Accordingly, our investigation focuses on the differences between the annealed and cold-rolled samples.

Further details of the samples and exposure conditions can be found in the IPPE report to LANL [1a] and [1b]. The exposed samples and unexposed control samples were received at UNLV from Los Alamos. We cut the samples to convenient sizes before analysis using abrasive cutoff wheels, cleaned the samples in methanol, and characterized the samples using a variety of tools: Scanning electron microscopy (SEM), energy-dispersive X-ray analysis (EDAX), and X-ray photoelectron spectrometry (XPS).

Our XPS instrument is a Surface Science Instruments SSX-100 which has been fitted with a Nonsequitur Technologies Model 1401 ion gun for sputtering. The XPS binding analyses were referenced to the adventitious carbon 1s line at 284.6 eV. The X-ray source for the XPS was a monochromatized and refocused aluminum $K\alpha$ (1486 eV) source with a 0.5–1.0 mm diameter X-ray spot size. The SEM was a JEOL JSM-5600 with an Oxford EDS detector. [1]

[1] EDX lines between 5–10 keV were used to characterize Fe and Cr in these sample. Interference from Pb and Bi is expected to be small, since independent XPS analysis indicates less than one atom percent of Pb and Bi on the surface.

4. Theory: basic mechanism of corrosion

The corrosion of steel by oxygen-controlled LBE is a complex phenomenon, involving both oxidation of the steel and dissolution of the steel into the LBE. Oxide formation rates are expected to decrease with time, due to mass transport considerations. (In some cases [e.g., [1f]], the thickness of the oxide layer grows as the square root of the time, following Wagner's law [9]). In contrast, the rate of dissolution from the surface of the oxide is constant in time (controlled by temperature, LBE flow rate, etc.). At long times, the oxide thickness should approach steady state: the growth rate of the oxide matches the dissolution rate, resulting in an oxide layer whose thickness is constant in time.

The LBE corrosion process may cause the sample to undergo either weight loss or weight gain, as found by Barbier and Rusanov [1f] or Gonzales [10], because in the first stages of corrosion, the sample initially gains weight by growing an oxide layer, but later loses weight as the sample dissolves in the LBE. Thus, weight change of the sample is an imperfect figure of merit to judge the extent of corrosion.

One of the most predictive of the current theories is the work of Ning Li [1c], who start with the observation that for a (metal) substrate to dissolve into an overlying liquid metal, it must be in the reduced (i.e., metallic) state. Thus, for a substrate oxide to dissolve, it must first be reduced to the metal and dissolved oxygen. Oxide can also be lost by mechanical processes (spallation). Using the thermodynamic stability of the oxides leads to a new equilibrium concentration of the (metal) substrate in the liquid LBE (in the surface stagnation layer). The new equilibrium concentration can be lowered by raising the dissolved oxygen concentration. With the addition of the diffusion equation and the effective thickness of the stagnant layer between the substrate wall and the fully mixed liquid, the corrosion rate can be found [1c]. Thus, oxygen control in LBE (limited at the upper end by the formation of PbO and at the lower end by formation of protective oxide) forces a lower corrosion rate by the formation of a more thermodynamically stable passivating oxide layer.

The gas-phase oxidation behavior of stainless steels, including 316 family steels, and the relevant oxide morphology, has been extensively reported in the literature [11]. In oxidation in air at elevated temperatures (0.13 atm. O_2, $T = 1273$ K) the oxide layer depends on the chromium content. At a chromium content of less than 2%, the oxide layer is pure iron oxide, while at chromium contents near 9%, an iron oxide layer is found above mixed iron and chromium oxides. At chromium contents of 16%, pitting corrosion is found with iron oxides over mixed iron/chromium oxide. At high (e.g., 28%) chromium content, a pure chromium oxide scale is found. The question naturally arises whether the insights

resulting from gas-phase oxidation of steels can be applied to the oxidation of steel in non-isothermal LBE loops. While the surface is definitely being oxidized, similar to the gas-phase case, in liquid metal the oxide is also being dissolved. Thus the results of this and similar studies are necessary for full understanding of the O/LBE/stainless steel system.

Many of the studies (e.g., Müller et al. [4]) of stainless steel in LBE found that the oxide at the surface of the steel was composed of an iron oxide (perhaps magnetite, Fe_3O_4), with an iron/chromium oxide layer (usually assumed to be a spinel) underneath. Li [1c] uses the commonly observed iron oxide surface layer to apply the theory to practical systems.

5. Results

5.1. SEM studies

Fig. 2 shows the SEM images of annealed and cold-rolled samples, and the changes caused by exposure to LBE. The annealed sample is shown in Fig. 2(a) (before exposure to LBE) and Fig. 2(b) (after exposure). The cold-rolled sample is shown in Fig. 2(c) (before exposure to LBE) and 2(d) (after exposure). The annealed sample (Fig. 1(a)) shows grain size of ~40 μm on etching. Fig. 1(b) shows the oxide surface on annealed 316/316L after 3000 h of exposure to LBE at 823 K. The oxide layer is thick, and does not reflect any underlying features. The cold-rolled sample (Fig. 1(c)) had an evident ~10 μm grain structure on the surface. The sample in Fig. 1(c) was not etched to enhance the grain structure. Fig. 1(d) shows the oxide surface on cold-rolled 316/316L after 3000 h of exposure to LBE at 823 K. The oxide layer is thin, and shows surface texture induced by cold-rolling.

5.2. EXAX studies

Fig. 3 shows EDAX spectra of the unexposed annealed (Fig. 3(a)) and unexposed cold-rolled (Fig. 3(b)) 316/316L samples. The peaks that are significant for elemental identification are at energies greater than 1 keV. Peaks below 1 keV are suffer from spectral congestion, overlap, and resulting ambiguous identification. The large peak at ca. 600 eV in Fig. 3(b), labeled Fe is probably oxygen. Disregarding the region below 1 keV, two figures are rather similar. The similarity of the figures show the composition of the two samples to be essentially similar, based on the average composition of the top few microns of the surface.

Fig. 4 shows EDAX spectra of annealed (Fig. 4(a)) and cold-rolled (Fig. 4(b)) samples, after 3000 h of exposure to LBE. Enhancement of chromium was

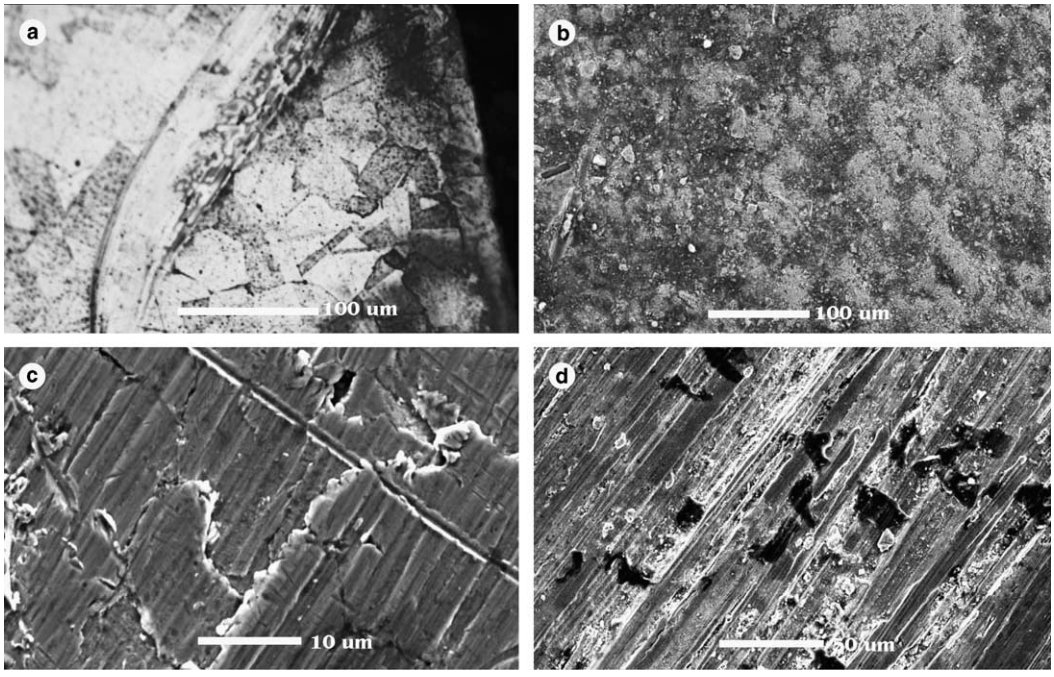

Fig. 2. SEM of 316/316L stainless steel samples, annealed and cold-rolled, before and after exposure to LBE. (a) unexposed annealed sample (cross section), (b) exposed annealed sample (surface), (c) unexposed cold-rolled sample (surface), (d) exposed cold-rolled sample.

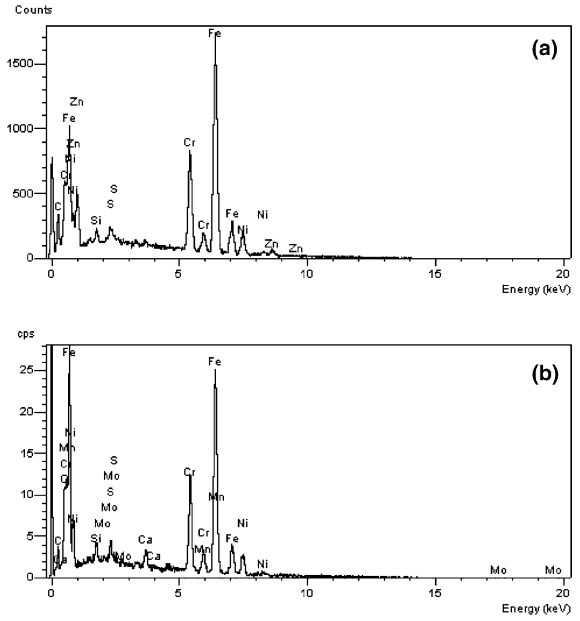

Fig. 3. EDAX of 316/316L before exposure to LBE (a) annealed (b) cold-rolled.

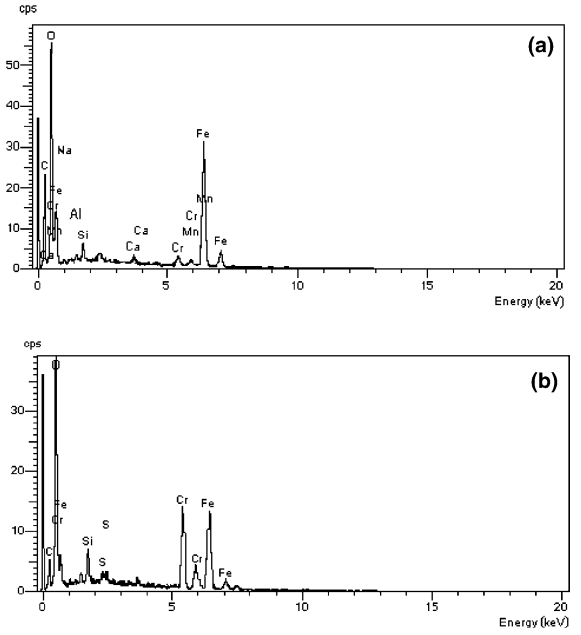

Fig. 4. EDAX of 316/316L after 3000 h of exposure to LBE (a) annealed (b) cold-rolled.

observed in the near-surface region of the cold-rolled sample (Fig. 4(b)), whereas the annealed sample (Fig. 4(a)) shows enhanced iron, compared to starting material.

5.3. XPS studies

XPS analyzes only the top few atomic layers, in contrast to EDAX which probes a deeper region. XPS data can be affected by a surface contamination of aliphatic carbon, arising from handling, atmosphere, etc. In order to eliminate this effect, the surface was examined before and after brief argon ion sputtering. The large oxygen and carbon component in the top few atomic layers make it necessary to look at ratios rather than absolute values of the surface atomic percentage of the components of interest (Table 1). Table 1 also shows the nominal electron binding energy of the elements whose peaks appear in the XPS spectra.

Fig. 5 shows XPS survey spectra of samples exposed to LBE, examining all peaks with binding energies in range 0–1100 eV, of 316/316L steel samples, before and after 85 s of argon ion sputtering. Fig. 5(a) is the annealed sample, while Fig. 5(b) is the cold-rolled sample. The peaks in these figures can be identified from the peak energies in Table 1.

The surface composition examined by XPS (Fig. 5) reveals some differences between the exposed annealed and exposed cold-rolled samples. The cold-rolled sample surface, Fig. 5(b), is enhanced in chromium (Fe/Cr = 1.8) with respect to the annealed sample (Fe/Cr = 3.3), Fig. 5(a).

Table 1
Composition of steel samples (atom percent), before and after exposure to LBE, as measured by XPS analysis after 85 s of argon ion sputtering

Sample	Exposure	Fe	Ni	Cr	Co	O	C	Pb	Bi	Mo
	BE (eV)	710	870	576	780	530	284	138	157	509
Annealed	unexposed	36	14	11	7	7	25	–	–	–
Cold-rolled	unexposed	16	24	9	7	17	23	–	–	2
Annealed	823 K, 3000 h	13	–	2	4	34	45	<1	<1	–
Cold-rolled	823 K, 3000 h	16	–	6	2	38	31	<1	<1	5

BE = nominal binding energy (eV). The binding energy allows peaks in the XPS spectra to be identified.

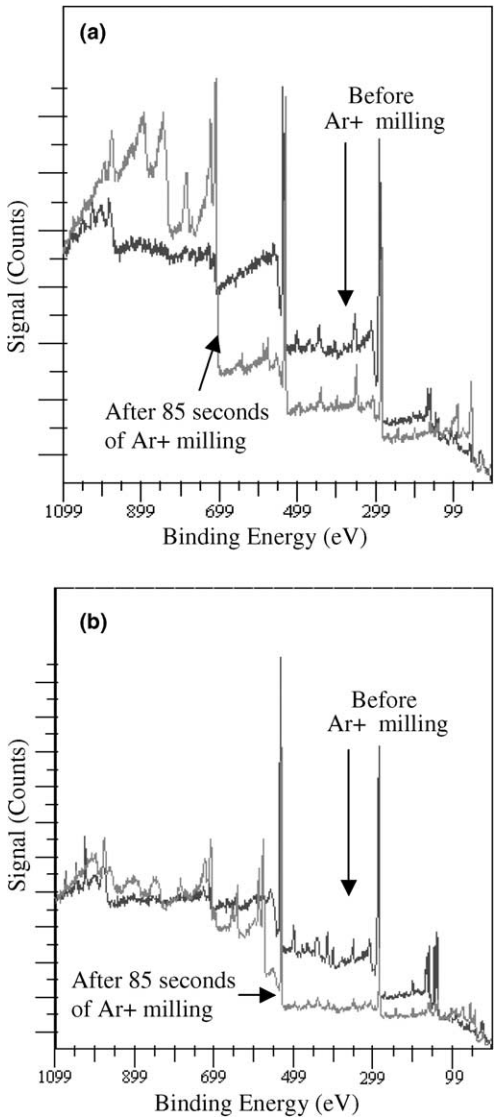

Fig. 5. (a) Characteristic XPS survey spectra of exposed annealed 316/316L sample before and after 85 s of argon ion sputtering. The source is monochromatized aluminum $K\alpha$ X-rays at 1486 eV. (b) Same as 2(a) but cold-rolled sample.

After exposure to oxygen-controlled LBE at 823 K for 3000 h, and 85 s of sputtering, the surface of the annealed sample is primarily iron oxide (Fe/Cr = 6.5), whereas the cold-rolled sample had large chromium content (Fe/Cr = 2.7). The present data cannot distinguish between the various iron oxides (e.g., Fe_2O_3 and Fe_3O_4).

While there is still large carbon contamination, the residual lead and bismuth concentration fall below one atom percent in both cases, indicating that there is little to no penetration of the LBE into the oxide layers. The exposed samples showed no nickel in the XPS, in agreement with previous work and the high solubility of nickel in LBE. We assume that the nickel has dissolved in the LBE.

Examination of the peak shape and location of the carbon and chromium core levels gives further information. Peak positions are referenced to the common aliphatic carbon peak (284.6 eV) found on as-received samples. The different binding energies of chromium (both Cr III and Cr VI) and their oxidation state dependent spin-orbit splittings are described by Perry et al. [12]. The binding energies of other elements are found in the standard NIST database [13].

All samples were lightly (5 s) argon ion sputtered to remove the majority of the overlying carbon. The carbon in the unexposed samples exhibited primarily a single peak (taken to be at 284.6 eV) except for the case of annealed unexposed sample, which showed a small carbide peak at 282.9 eV, consistent with chromium carbide (Fig. 6(a)).

The chromium in the unexposed annealed sample (Fig. 6(b)) exhibited a Cr $2p_{3/2}$ line at 574.7 eV and a spin-orbit splitting of the Cr $2p_{3/2,1/2}$ of 9.2 eV, consistent with metallic and/or carbidic chromium. The asymmetric broadening of the two main photoelectron lines can be attributed minimally to higher binding energy satellite structure hidden in the shoulder of the lines and also, possibly, to charging effects due to the non-conducting nature of the surface. Additionally, the broadening may also be due to a small inclusion of other partially oxidized chromium species and/or lack of crystallinity of the chemical species on the surface. The chromium spectra of the unexposed, cold-rolled sample (Fig. 6(b)) show chromium at a binding energy and splitting consistent with those of Cr_2O_3 (a Cr $2p_{3/2}$ binding energy value of 576.6–576.8 eV and a splitting of 9.7–9.9 eV). The spectra of the exposed cold-rolled and exposed annealed samples (not shown) are also consistent with Cr_2O_3.

The unexposed annealed and unexposed cold-rolled samples are dramatically different. The annealed sample shows metallic or carbidic chromium and carbidic carbon, whereas the cold-rolled sample shows chromium oxide and the absence of carbidic carbon. This indicates a lower stability of chromium oxide on the annealed sample than on the cold-rolled sample. Since chromium oxide is the preferred passivating oxide layer, this observation on the unexposed samples presages the oxide composition on the exposed samples. On extended sputtering (85 s), a carbide peak was found for both annealed and cold-rolled unexposed samples, presumably due to ion beam induced reaction between the chromium and the residual carbon.

5.4. Sputter depth profiling XPS studies

We undertook a sputter depth profiling study to determine the overall oxide compositional morphology.

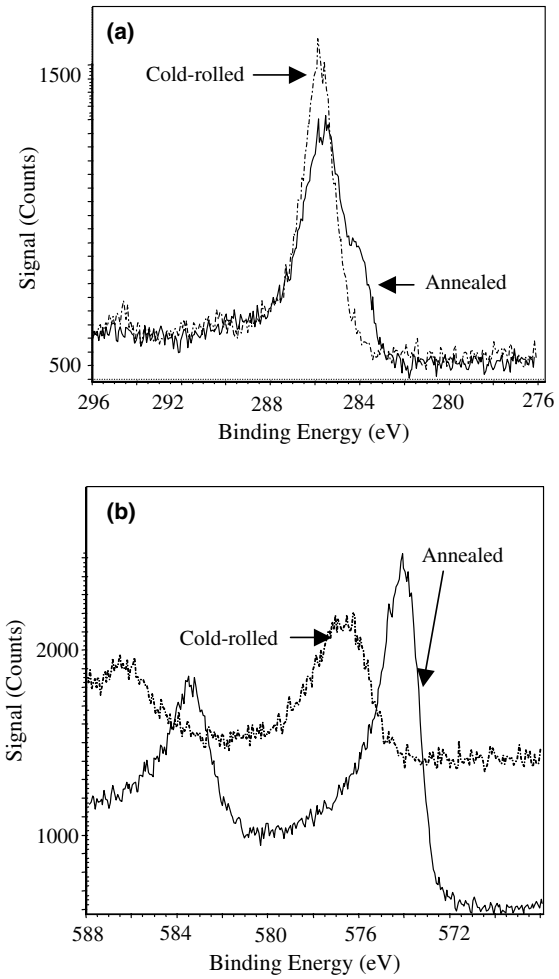

Fig. 6. (a) Comparison of high-resolution XPS spectra of unexposed annealed and cold-rolled samples in the carbon region. Note the evidence of carbidic carbon in the annealed sample. (b) Same as 3(a) but the chromium region. Note the evidence of chromium oxide in the cold-rolled sample. The electron binding energy scale has not been corrected for charging of the sample. The binding energies cited in the text have been corrected for charging, by referencing the alphatic carbon peak at 284.6 eV.

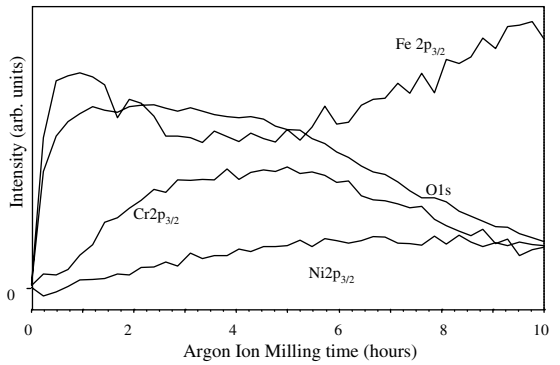

Fig. 7. Depth profile of annealed 316/316L after exposure to LBE for 1000 h at 823 K. Total sputter depth is ~30 μm. Note enhancement of iron and oxygen at the surface and the depletion of chromium. The composition of the 3000 h, 823 K sample (not pictured) was similar, with more iron to be found in the underlying Fe/Cr mixed oxide layer.

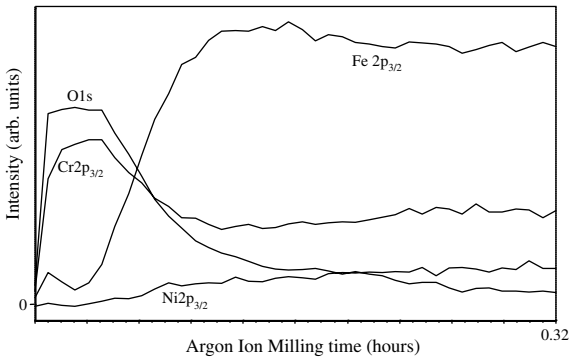

Fig. 8. Depth profile of cold-rolled 316/316L. Total sputter depth is ~1 μm. Note that initial chromium oxide surface is preserved over metal surface. Only a small amount of surface iron oxide is present. The composition of the 3000 h, 823 K sample (not pictured) was similar, with slightly more iron to be found in the primarily chromium oxide layer.

While the very long sputtering times (up to 10 h) alters the detailed chemical composition of the surface, elemental analysis is still useful.

The sputter depth profiles of annealed and cold-rolled samples show marked differences (Figs. 7 and 8). The oxide on the annealed exposed sample has a top layer of iron oxide over a layer of mixed chromium and iron oxides (either a mixed oxide or a spinel). We observed that the total oxide thickness on the annealed sample was ~30 μm, based on SEM measurements and the sputter rate. The cold-rolled sample had an oxide thickness of ~1 μm, based on similar information. Our results for the oxide thickness are consistent with the Russian results mentioned above. The cold-rolled sample showed a surface chromium oxide layer, with a possible mixed chromium/iron oxide underneath, whereas the annealed sample showed iron oxide at the surface, with a clear mixed oxide underneath.

One complicating factor is the variation in the thickness of the oxide layer from one point to another in the sample. This factor affects the measurement of the elemental composition of the bottom of the oxide layer, because experimental measurements are combinations of the signals from the oxide layer (in regions where the oxide layer is thicker) and from the bulk material (in regions where the oxide layer is thinner). This complicating factor does not affect the measurement of the elemental composition of the top of the oxide layer.

The results for the samples exposed to LBE at 823 K for 3000 h show the same morphology as the 1000 h samples, with the observation of an increase in the iron percentage in the mixed layer in the annealed sample and the chromium layer in the cold-rolled sample. These shifts may be due to a slow dissolution of the underlying iron into the passivating oxide layer.

Our SEM and EDAX results are consistent with previous work, as discussed below in detail. Our XPS results confirm the oxide bilayer for annealed 316/316L and show that the cold-rolled oxide is much closer to pure Cr_2O_3 than the annealed sample. Further, the surface of the unexposed cold-rolled sample was found to be systematically more oxidized than the annealed sample.

6. Discussion

In the present work, we find that a cold-rolled 316/316L sample forms a protective chromium oxide layer while under identical conditions an equivalent annealed 316/316L sample forms a thicker, less protective oxide, consisting of two layers: an inner layer of mixed iron and chromium oxides and an outer layer of iron oxide.

This result appears surprising at first glance: cold-rolling creates stressed and defective surface layers. These additional defects and grain boundaries could be expected to increase the rate of oxidation, and hence corrosion, by allowing more rapid oxygen diffusion, greater galvanic/stress corrosion, more deleterious inclusion formation, and the creation of poorer quality protective oxide layers.

The conventional wisdom associating grain boundaries with corrosion is well-established [14]. For example, a well-known deleterious effect of grain boundaries is the precipitation of chromium carbides or chromium/molybdenum carbides, producing a near-surface layer that is depleted in free chromium and therefore unable to form a passivating chromium oxide layer.

Our results are that cold-working leads to lower corrosion rates. Cold-rolling introduces three changes: it reduces grain size and creates other lattice defects in the near surface layer, it often creates surface textures (rolling marks), and it creates a very deformed surface layer of metal.

In high-temperature corrosion, small grain sizes have been associated with greater corrosion resistance, for two possible reasons: (1) the key limiting factor in the formation of a protective oxide layer of Cr_2O_3 is the availability of chromium at the surface. Often, chromium cannot migrate rapidly enough from the bulk to the surface to form a protective oxide layer. Grain boundaries provide paths of rapid diffusion for chromium. Hence, more grain boundaries help in the formation of a protective oxide layer. Cold-rolled samples, with more grain boundaries per unit surface area than annealed samples, are therefore more resistant to corrosion. (2) Chromium oxides initially form in the grain boundary region, and then diffuse laterally. If they merge to form a continuous chromium oxide film, the result is corrosion resistance. In a sample with smaller grain size, the distance to be traveled from the grain boundaries is less. Hence a small-grain sample is more likely to form a continuous protective oxide film [15–18].

Cold working has also been implicated in an earlier transition from internal oxidation to the formation of a protective surface oxide [19,20].

The other effects of cold working, textures and the highly deformed surface layer, have not been as intensely investigated. Textures might help anchor the protective oxide against thermal/mechanical degradation, and subsequent formation of patches of inferior oxide (as seen in previous work e.g. [4]). The highly deformed surface layer may easily form an initial oxide layer, which might lead to a more orderly formation of a subsequent protective oxide, as has been suggested for Fe–Cr–Al alloys [21].

7. Conclusions

The present work is an investigation into the effects of surface preparation on LBE corrosion. Analysis of the samples shows that the cold rolled sample has a thin, primarily chromium oxide layer on the surface, which protects the sample from corrosion during LBE exposure. The annealed sample has a thicker oxide layer, consisting of an outer layer enhanced in iron but depleted in chromium, and an inner layer with both iron and chromium. It is very encouraging to note that under the right circumstances (e.g., right surface preparation), a persistent chromium oxide layer can be obtained and stabilized on commercial 316-class steels, potentially making possible the operation of lead-alloy systems (transmuters, reactors, spallation sources, etc.) with a higher operating temperature and a low corrosion rate with existing materials.

Acknowledgements

This work is funded through the University of Nevada, Las Vegas Transmutation Research Program administered through the Harry Reid Center for Environmental Studies under the following US Department of Energy contracts: Advanced Fuel Cycle Program grant no. DE-FG04-2001AL67358 and DE-AC03-76SF00098. This work was supported by the Office of Nuclear Energy, Science, and Technology, US Department of Energy, under the auspices of the Transmutation

Research Program at the University of Nevada, Las Vegas. We gratefully acknowledge Eric Loewen for editorial assistance and Lindsay Wylie for assistance with the figures.

References

[1] (a) A. Rusanov et al., Report for Contract #H12030008-35, SSC RF IPPE (Russia), Los Alamos National Laboratory (USA), 2000;
(b) N. Li, X. He, A. Rusanov, A.P. Demishonkov, Proceedings of AccApp'01, 11–15 November 2001, Reno, NV, USA
(c) N. Li, J. Nucl. Mater. 300 (2002) 73;
(d) F. Barbier, G. Benamati, C. Fazio, A. Rusanov, J. Nucl. Mater. 295 (301) 149;
(e) H. Glasbrenner, J. Konys, G. Mueller, A. Rusanov, J. Nucl. Mater. 296 (2001) 237;
(f) F. Barbier, A. Rusanov, J. Nucl. Mater. 296 (2001) 231.
[2] E.P. Loewen, H.J. Yount, K. Volk, A. Kumar, J. Nucl. Mater. 321 (2003) 269.
[3] G. Benamati, C. Fazio, H. Piankova, A. Rusanov, J. Nucl. Mater. 301 (2002) 23.
[4] G. Müller, A. Heinzel, J. Konys, G. Schumacher, A. Weisenburger, F. Zimmermann, V. Engelko, A. Rusanov, V. Markov, J. Nucl. Mater. 301 (2002) 40.
[5] C. Fazio, I. Ricapito, G. Scaddozzo, G. Benamati, J. Nucl. Mater. 318 (2003) 325.
[6] H. Glasbrenner, F. Groschel, T. Kirchner, J. Nucl. Mater. 318 (2003) 333.
[7] S. Guerin, J.-L. Pastol, C. Leroux, D. Gorse, J. Nucl. Mater. 318 (2003) 339.
[8] K. Kikuchi, Y. Kurata, S. Saito, M. Futakawa, T. Sasa, H. Oigawa, E. Wakai, K. Miura, J. Nucl. Mater. 318 (2003) 348.
[9] A. S. Khanna, Introduction to High Temperature Oxidation and Corrosion, ASTM, Materials Park, OH 44073, 2002, p. 9.
[10] M.M. Gonzales, Biotechnol./Pharm. Facil. Des. (2001) 2.
[11] J.R. Davis, Carbon and Alloy Steels, ASM International, Materials Park, OH, 1996, p. 510 (Table 1);
R.C. Lobb, H.E. Evans, Corr. Sci. 23 (1983) 55;
D.P. Whittle, G.C. Wood, D.J. Evans, D.B. Scully, Acta Metall. 15 (1967) 1747.
[12] D.L. Perry, L. Tsao, J.A. Taylor, Inorg. Chim. Acta 85 (1984) L57, and references therein.
[13] NIST on-line database (http://srdata.nist.gov/xps/).
[14] D. Talbot, J. Talbot, Corr. Sci. Technol, CRC, 1998, p. 275.
[15] D.R. Baer, Appl. Surf. Sci. 7 (1981) 69.
[16] D.R. Baer, M.D. Merz, Metall. Trans. A 11A (1980).
[17] H.J. Grabke, Surf. Interface Anal. 30 (2000) 112.
[18] C.S. Giggins, F.S. Pettit, Trans. Metall. Soc. AIME (1969).
[19] F.H. Stott, Mat. Sci. Technol. 5 (1989) 734.
[20] R.A. Rapp, Corrosion 21 (1965) 382.
[21] J.D. Rawers, E.M. Mattlin, Metall. Trans. A 18A (1987) 1805.